Production of bulk solid-state PEI nanofoams using supercritical CO_2

Brian Aher, Nathan M. Olson, and Vipin Kumar[a)]
Mechanical Engineering Department, University of Washington, Mechanical Engineering Building, Stevens Way, Seattle, Washington 98195

(Received 11 February 2013; accepted 26 March 2013)

In this paper, a process to introduce nanoscale cells in homogeneous polyetherimide (PEI) is presented. The nanofoams produced have a bulk porosity (void fraction) in the range of 25–64%, with the average cell sizes in the range of 40–100 nm. Uniform nucleation of cells throughout the volume of the PEI specimen was observed. Supercritical CO_2 at 20 MPa was used as the blowing agent and the specimens were foamed in a hot press to ensure flatness for further processing and characterization. Sorption studies showed that at 20 MPa, PEI can absorb about 10% CO_2 by weight and that a 1-mm thick specimen can reach an equilibrium concentration in approximately 100 h at 45 °C. The effects of desorption time, foaming temperature, clamping pressure, and foaming time were investigated. Several nanoscale morphologies were observed through changes in the foaming temperature, which ranged from 165 to 210 °C. In one experiment, it was found that when the clamping force is increased from 1 to 10 tons, the average cell size increased from 40 to 4000 nm or by a factor of 100. This points to the clamping force as an important process variable to control the nanostructure introduced in PEI. Optimal processing conditions for the production of defect-free nanofoams are presented.

I. INTRODUCTION

Microcellular foams (having cells in the order of 10 μm) and nanocellular foams (having cells <1000 nm) have been produced in a wide range of polymers. These foams are of interest because of their potential for novel properties that are highly dependent on morphology and can differ greatly from the bulk material.[1–3] Some properties that may be enhanced in micro- and nanofoams are thermal conductivity,[4] specific strength and toughness,[5,6] and dielectric constant.[7,8]

These properties have made polymer microfoams and nanofoams attractive for use in packaging materials, insulation, sports equipment and automobile parts,[9] liquid crystal and plasma displays,[10] and thin film microelectronics.[11] High temperature polymeric foams have been proposed for aircraft structures.[12] Open nanofoams have applications in controlled release systems,[13] porous membranes,[14] and ion exchange applications such as battery separators.[15]

The solid-state foaming process was originally developed at Massachusetts Institute of Technology[16,17] in 1984, using nitrogen as the blowing agent to create microcellular polystyrene foam. The process has been extended to many amorphous and semicrystalline polymers, including polymethylmethacrylate (PMMA),[18] polyvinyl chloride,[19] polycarbonate,[20] acrylonitrile–butadiene–styrene,[21] polyethylene terephthalate,[22] crystallizable polyethylene terephthalate,[23] and polyactic acid.[24] The first step in the foaming process is saturation of the polymer with a dissolvable gas. In the second step, bubbles are nucleated by reducing the solubility of the gas in the polymer by either a sudden drop in pressure[25] or a sudden increase in temperature.[19,20] The process is called "solid-state" because the temperature required for bubble nucleation is less than the glass transition temperature of the polymer due to the plasticizing effect of the dissolved gas.[26]

Polymer nanofoams have been produced using the block copolymer method[27,28] or by the use of nanocomposite additives such as nucleation sites.[29] The solid-state process was used to create nanofoams in polyetherimide (PEI) and polyethersulfone (PES) by Krause[13,30] who reported 200 nm cells in thin films. The process was extended to bulk materials by Miller[10] who investigated the influence of saturation pressure on cell morphology and the effect of cell morphology on impact and tensile strength.[31]

The use of supercritical CO_2 as a blowing agent has been increasingly popular,[32,33] largely due to its increased diffusion rate, which allows a shorter saturation time.[34] Huang[18] used supercritical CO_2 to produce nanofoam in PMMA. Sorrentino[35] used supercritical CO_2 to produce nanofoams in poly(ethylene-2,6-naphthalate), PES, polyphenylsulfone and PEI. Zhou et al.[34] presented a process map of the cell morphology of PEI micro- and nanofoams produced using supercritical CO_2 and reported their mechanical and thermal properties.

Our interest in the PEI-CO_2 system is due to the wide range of cell sizes (40 nm to >4000 nm) that can be created using the solid-state process under different conditions.

a)Address all correspondence to this author.
e-mail: vkumar@uw.edu
DOI: 10.1557/jmr.2013.108

 © Materials Research Society 2013

https://doi.org/10.1557/jmr.2013.108 Published online by Cambridge University Press

We are interested in producing flat samples of open nanofoams for further investigations into filtration and ion exchange applications. In this study, we investigate the effects of desorption time, foaming time, foaming temperature, and clamping pressure on the cellular morphology and bulk density of PEI nanofoam.

II. EXPERIMENTAL METHOD

Commercially available sheets of PEI were used for these experiments. The sheets consist of 1.016 mm (0.040″) thick Ultem® 1000 (SABIC Innovative Plastics, Pittsfield, MA) obtained from McMaster-Carr. The sheets have an initial glass transition temperature of 215 °C and a density of 1.27 g/cm^3 and are free of additives. The chemical structure of PEI is shown in Fig. 1. Samples were cut into 45 × 45 mm squares.

A supercritical CO_2 pressure vessel system was used for saturating the PEI samples. This system consists of a high-pressure steel vessel connected to a Teledyne Republic/Sprague S-86-JN gas booster (Sprague Products, Brecksville, OH). The gas booster uses compressed air to drive a pump that pressurizes the vessel above the CO_2 source pressure. This system utilizes an Omega process controller to regulate the pressure inside the vessel. The pressure vessel also has an external heating pad controlled by a Cole-Parmer Digi-Sense 89000-00 temperature controller unit. This unit uses a thermocouple located on the inside of the vessel to monitor the saturation temperature. This apparatus was used for saturating PEI samples at 20 MPa and 45 °C for at least 72 h before removal for desorption and foaming. The concentration of the dissolved gas in the polymer sample is measured by weight on a Mettler AE240 balance (Mettler-Toledo LLC, Columbus, OH) and reported as a percent of the original weight of the sample.

Saturated samples were foamed in a Wabash Genesis hydraulic press. The samples were desorbed at room temperature and pressure for a set amount of time prior to foaming. Samples were placed one at a time in the middle of the hot press platens, which were preheated to the desired foaming temperature. Each sample was held between four layers of polytetrafluoroethylene-coated fiberglass fabric. The top and bottom layers of the fabric were tightly woven fiberglass intended to allow for easy sample release from the platens. The layers immediately adjacent to the sample had a porous, open weaving that allowed excess CO_2 from the sample to be released during foaming. The hot press was set to close rapidly until it reached an adjustable point, set to be just thicker than the unfoamed sample. At this point, it closed slowly on the sample and raised the force up to a set point. This force and temperature were maintained for a set foaming time, after which the platens were opened and the sample was promptly removed. The clamping pressures presented in this paper are the clamping force divided by the area of the unfoamed sample. The samples were cooled at room temperature. The solid-state foaming process is shown in Fig. 2.

The foamed samples were characterized by measuring the density, cell size, solid skin thickness, and transition layer thickness. A cross-section of a typically foamed sample shows a core of nanoscale cellular structure with transition layers of microscale cells on the top and bottom, followed by a thin solid skin. The mass density was measured by displacement per ASTM D-792, using water as the liquid. A Mettler-Toledo AE240 balance and a laboratory wet/dry mass device were used to perform the density measurements. The reported density reflects the bulk density of the sample, including the solid skin layer and transition layer. The density is reported in this paper as relative to original density of the PEI samples.

Cell size, skin thickness, and transition layer thickness were measured by analyzing scanning electron microscope (SEM) images of the microstructure of the foams. SEM samples were prepared by liquid nitrogen freeze fracture and 60 s of Au/Pd deposition by an SPI sputter module controller. An FEI Sirion SEM (FEI, Hillsboro, OR) was used to obtain the images of the fracture surface. The cell size was determined from the images taken from the core region of each foam sample. The solid skin thickness was measured from the images taken at the edges of each sample. A series of lines perpendicular to the surface of the foam were drawn and the distance from the surface to the first cell intersected along each line was measured. Averaging these distances together yields an accurate depiction of the solid skin thickness for each

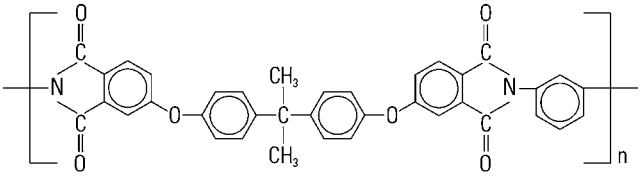


FIG. 1. Chemical structure of PEI.

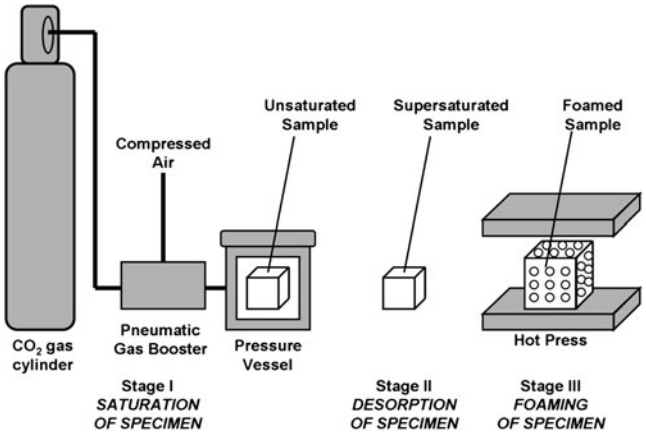


FIG. 2. Diagram of solid-state PEI foaming process.

https://doi.org/10.1557/jmr.2013.108 Published online by Cambridge University Press

sample. The microcellular transition layer appears darker in the SEM images than the nanocellular core. The transition layer thickness was determined by measuring the distance from the edge of the sample to the beginning of the lighter region and includes the solid skin thickness as reported.

The motivation for this investigation was to develop a method for reliably producing specimens for investigating solid skin removal from nanocellular foams. The goal was to be able to produce flat, nonblistered, nanocellular samples in a fast repeatable process. Four experiments were undertaken to investigate the use of press foaming PEI samples saturated under supercritical conditions. Each experiment sought to vary one process variable while keeping all others constant.

The first experiment focused on varying desorption time prior to foaming. Preliminary experiments suggested a significantly higher rate of internal blistering at lower desorption times. The internal blisters form around the midplane of the plastic sheet and expand perpendicularly to the clamp pressure. In extreme cases, the internal blisters can join and separate the sample into two halves attached only at the edges. One sample was foamed at each of the eight desorption times. The chosen desorption times were every 10 min from 5 to 75 min. The platen temperature was 195 °C and the clamping pressure was 2.2 MPa. Samples were held in the hot press for 3 min.

The second experiment focused on varying the temperature of the hot press platens during foaming. The selected temperatures were 165, 175, 185, 195, 205, and 210 °C. Three samples were foamed at each of the six selected temperatures for a total of 18 samples. A clamp pressure of 2.2 MPa and a foaming time of 3 min were used in this experiment. All samples were desorbed for between 60 and 90 min prior to foaming.

The third experiment focused on varying the clamping pressure. The clamping pressures selected for this study were 0.44, 2.2, 4.4, 22, and 44 MPa. One sample was foamed at each selected clamping pressure. The platen temperature was 195 °C. Samples were held in the hot press for 3 min. All samples were desorbed for between 88 and 107 min prior to foaming.

The final experiment focused on varying the foaming time. This is measured as the duration that the press holds the sample during foaming. The foaming times selected for this study were 0.5, 1, 1.5, 2, 2.5, 3, 3.5, 4, 4.5, 5, 7.5, and 10 min. One sample was foamed for each of the selected foaming times. The clamp pressure was set to 2.2 MPa and the platens were heated to 195 °C. Due to the long foaming times necessary, the samples were allowed to desorb for 60 min before being placed in a freezer set to 0 °C to retard further desorption. The samples were then removed two at a time and promptly foamed. The goal was to minimize the difference in desorption between all of the samples.

III. RESULTS AND DISCUSSION

A. Sorption

The sorption rate of CO_2 in PEI was investigated using supercritical saturation conditions of 20 MPa and 45 °C. Figure 3 shows the sorption behavior of two samples of PEI under these conditions. Measurements were taken approximately 2 min after pressure release, and thus reflect some desorption of gas from their initial state. Samples in this study were considered saturated after 72 h of sorption, showing a final concentration >11% by weight. Figure 4 shows the measured desorption behavior of two saturated samples, desorbed at room temperature and 0 °C. A constant diffusion coefficient D was calculated by fitting the desorption data to the equation[36]

$$\frac{M_t}{M_\infty} = 1 - \sum_{n=0}^{\infty} \frac{8}{(2n+1)^2\pi^2} \exp[-D(2n+1)^2\pi^2 t/4l^2] \quad ,$$

where M_t is the mass of CO_2 that has left the sample at time t, M_∞ is the mass of CO_2 in the saturated sample, and l is the thickness of the sample. The diffusion coefficients thus calculated were $D = 2.52 \times 10^{-8}$ cm^2/s at 23 °C and $D = 1.08 \times 10^{-8}$ cm^2/s at 0 °C. These diffusion coefficients are only valid when the samples are nearly saturated because the diffusion coefficient is heavily dependent on the concentration. The 11.3% weight concentration in the saturated samples matches well with the empirical model of Zhou,[34] which predicts an equilibrium concentration of 11.2% at 20 MPa and 45 °C.

B. Desorption

Figure 5 shows the results of varying desorption time prior to foaming the sample in the press between 5 and 75 min. All samples foamed after <35 min of desorption contained considerable internal blistering. Samples foamed after 35 or more minutes contained no internal blisters but had thicker transition layers. The solid skin remained between 10 and 20 μm thick, whereas the transition layer grew steadily from 54 μm after 5 min of desorption to

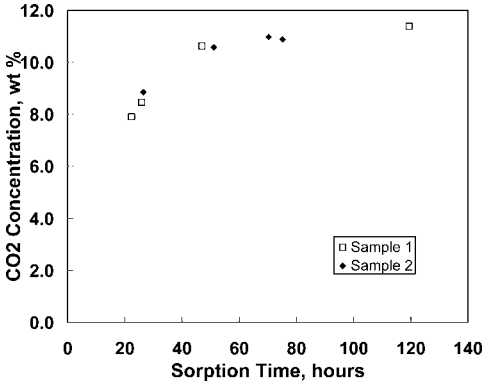


FIG. 3. Weight fraction of CO_2 in two 1.016 mm thick PEI samples, saturated at 20 MPa and 45 °C.

https://doi.org/10.1557/jmr.2013.108 Published online by Cambridge University Press

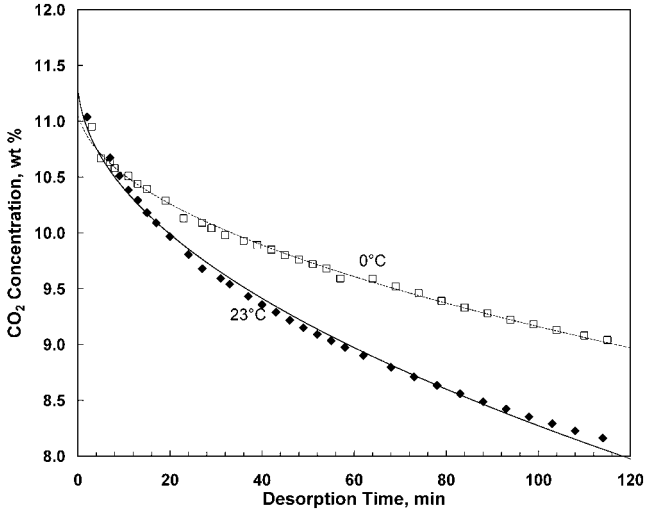


FIG. 4. Weight fraction of CO_2 in two 1.016 mm thick PEI samples, desorbed at 0 °C and 23 °C. The curves are the weight fraction of CO_2 assuming a constant diffusion coefficient.

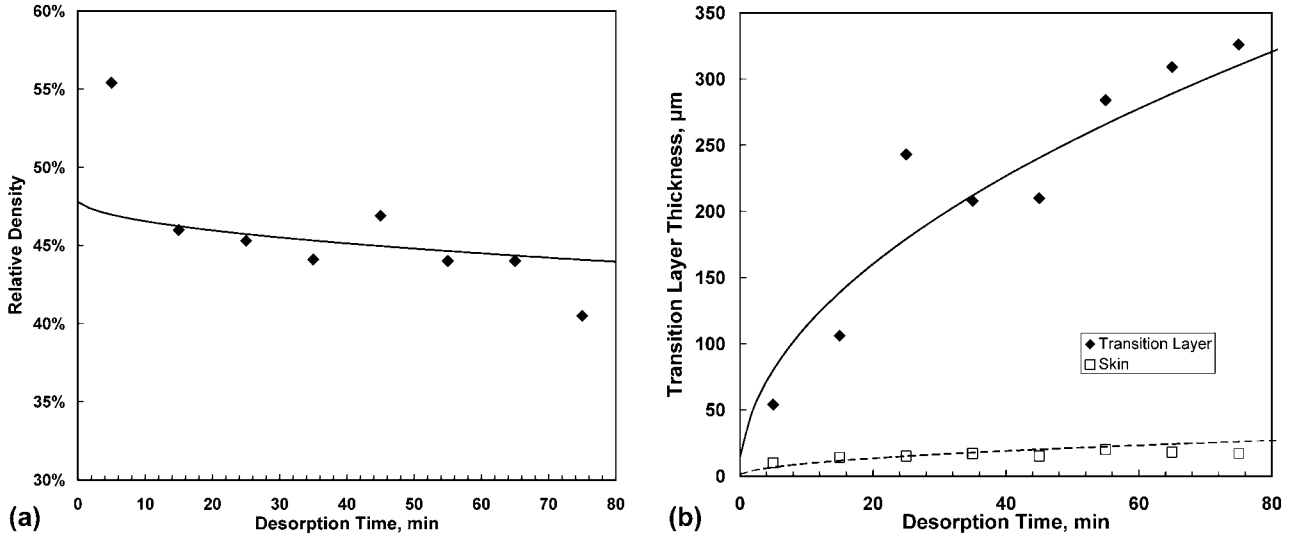


FIG. 5. (a) Relative density of samples foamed for 3 minutes at 195 °C, 2.2 MPa clamping pressure, at various desorption times, and (b) Thickness of microcellular transition layer and skin of samples foamed for 3 minutes at 195 °C, 2.2 MPa clamping pressure, at various desorption times. The curves are based on a constant diffusion coefficient and an 8.5% CO_2 concentration threshold for nanocellular foaming.

326 μm after 75 min of desorption. This effect is due to the diffusion of CO_2 out of the sample. The locally lower gas concentration near the surface leads to the development of fewer and larger cells. Thus, more desorption leads to a thicker transition layer. Figures 6 and 7 show SEM images of the two samples foamed after different desorption times. The average size of the transition layer cells closest to the skin was 4 μm.

The relative density of the samples decreased with increasing desorption time. This can be explained by considering the samples as consisting of three materials (the core, transition layer, and skin), each with its own characteristic density but present in differing amounts. The rule of mixtures gives

$$t_f \rho_f^* = 2t_s \rho_s^* + 2t_t \rho_t^* + t_c \rho_c^* \quad ,$$

where ρ* is the relative density, t is the thickness, and the subscripts f, s, t and c refer to the overall foam, skin, transition layer, and core respectively. The factors of two multiplied with the skin and transition layer terms are due to the fact that each sample is symmetric and has two skins and two transition layers. The skin was assumed to have a relative density of $\rho_s^* = 1$, leaving ρ_t^* and ρ_c^* as free parameters that were fit to the observed parameters ρ_f^*, t_f, t_s, t_t, and t_c. Using this technique, the relative density of the transition layer was estimated to be 32%, and the relative density of the core was estimated to be 48%.

https://doi.org/10.1557/jmr.2013.108 Published online by Cambridge University Press

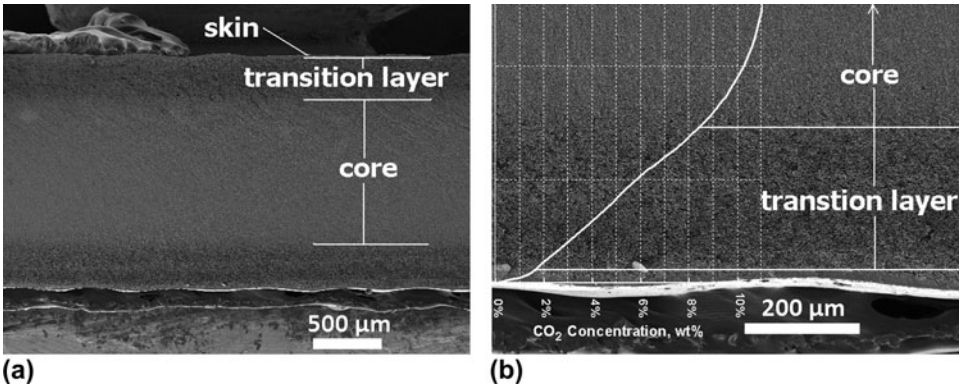


FIG. 6. (a) SEM of typical nanocellular PEI sample cross-section, showing nanocellular core, transition region, and solid skin, and (b) SEM of the microcellular transition layer, with graph of CO_2 concentration at foaming. The sample was foamed for 3 minutes at 195 °C, 2.2 MPa clamping pressure, after desorbing for 65 minutes.

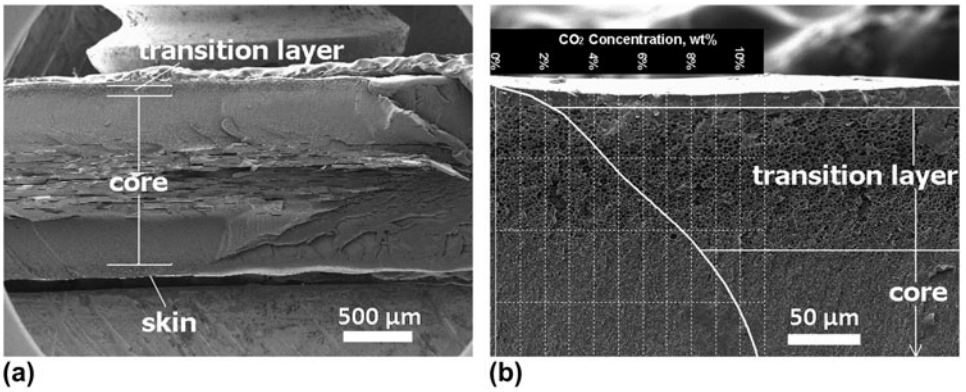


FIG. 7. (a) SEM of nanocellular PEI sample cross-section showing internal blistering, and (b) SEM of the mircrocellular transition layer, with graph of CO_2 concentration at foaming. The sample was foamed for 3 minutes at 195 °C, 2.2 MPa clamping pressure, after desorbing for 15 minutes.

The importance of estimating these densities is that it allowed us to map locations in the foamed sample back to the locations in the unfoamed sample in which the CO_2 concentration is known as a function of time. Assuming the in-plane growth of the sample is equal among all three layers

$$t_f^* \rho_f^* = t_s^* \rho_s^* = t_t^* \rho_t^* = t_c^* \rho_c^* \quad ,$$

where t^* is the ratio of thickness of a layer in the foamed sample to thickness of the layer in the unfoamed sample. The out-of-plane expansion of each layer was assumed to be uniform throughout its thickness. This procedure, shown in Fig. 8, was used to provide an estimate for the threshold CO_2 concentration at which the structure becomes nanocellular. At this foaming condition, the threshold CO_2 concentration is approximately 8.5%.

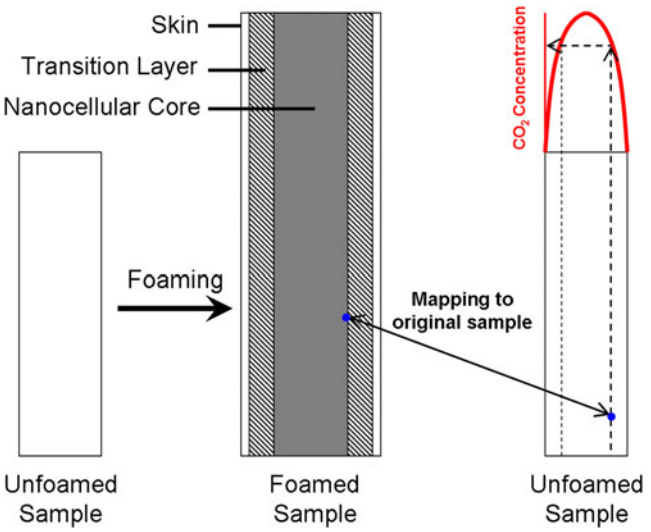


FIG. 8. Process for estimation of threshold CO_2 concentration for nanocellular foaming. The boundary between nanocellular and microcellular regions is mapped back into the unfoamed sample, where the CO_2 concentration is known. The pre-foaming CO_2 concentration at this boundary is the threshold for nanocellular foaming.

C. Foaming temperature

Figure 9 shows the range of relative densities and cell sizes achieved with various foaming temperatures. The relative density decreases with increasing foaming temperature

https://doi.org/10.1557/jmr.2013.108 Published online by Cambridge University Press

until reaching a lower limit of 43.9% at 195 °C. The relative density rises dramatically between 205 and 210 °C. This effect is likely due to collapse of the cellular structure under the hot press pressure and temperatures near the glass transition. The samples foamed at 210 °C were significantly reduced in thickness after foaming, whereas all others gained thickness. Figure 10 illustrates the different cellular structures obtained at various foaming temperatures.

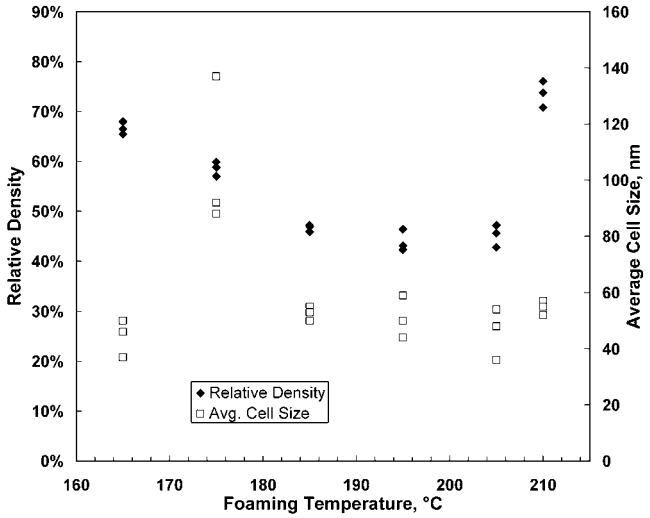


FIG. 9. Overall relative density and average core cell size of samples foamed for 3 minutes with 2.2 MPa clamping pressure, at various temperatures.

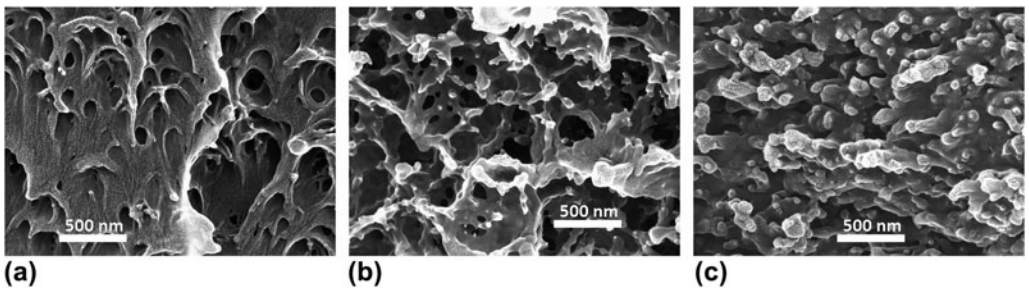


FIG. 10. SEM of core structure of samples foamed for 3 minutes with 2.2 MPa clamping pressure, at (a) 165 °C, (b) 195 °C, and (c) 210 °C.

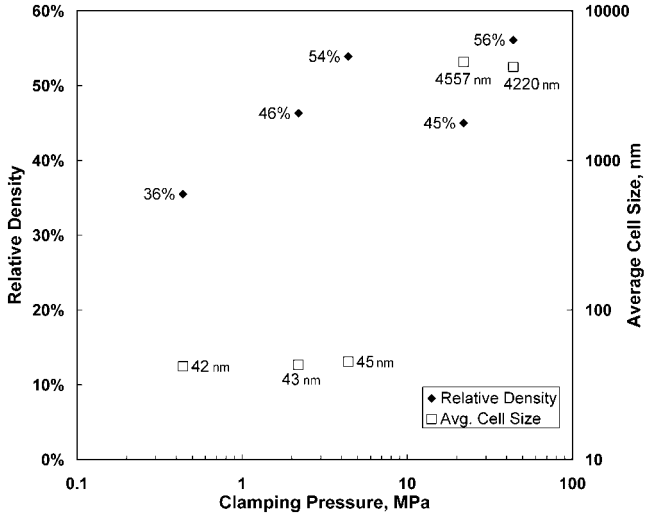


FIG. 11. Overall relative density and average core cell size of samples foamed for 3 minutes at 195 °C, at various clamping pressures.

https://doi.org/10.1557/jmr.2013.108 Published online by Cambridge University Press

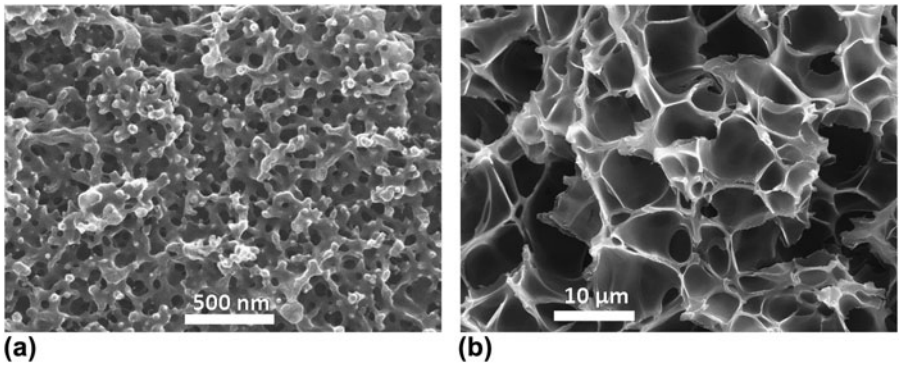


FIG. 12. SEM of core structure of PEI samples foamed for 3 minutes at 195 °C, and (a) 0.44 MPa clamping pressure (b) 22 MPa clamping pressure.

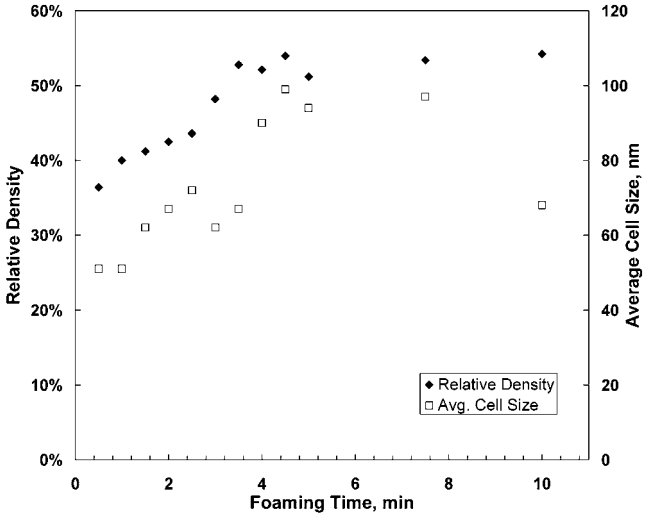


FIG. 13. Overall relative density and average core cell size of samples foamed for various times at 195 °C, 2.2 MPa clamping pressure.

D. Clamping pressure

Figure 11 shows the range of relative densities and cell sizes achieved with various clamping pressures. Between 4.4 and 22 MPa, there was an abrupt transition from a nanocellular structure to a microcellular structure, with the cell size increasing by two orders of magnitude. In the nanocellular regime, increasing the clamping pressure led to an increase in the relative density. Figure 12 illustrates the different cellular structures obtained at different clamping pressures.

E. Foaming time

The effect of longer foaming time in the traditional microcellular batch process is an increase in the cell size as nucleated cells absorb gas from the surrounding polymer matrix and grow as well as a corresponding decrease in the relative density. Figure 13 shows a similar trend of increasing average cell size with longer foaming times with samples foamed in the hot press. Conversely, Fig. 13 shows a clear trend of increasing relative density with increased foaming time. This is likely due to the clamping pressure not allowing free growth of the sample during foaming. The lowest average cell size achieved in this investigation was 51.8 nm in a sample foamed for just 30 s, with a relative density of 36.4%. However, sample flatness is one of the key goals of this process. Samples foamed for <3 min had a significant curvature, whereas all samples foamed for 3 min or longer were flat. This may be due to the relaxation of internal stresses resulting from the foaming process that would otherwise cause warping upon cooling.

IV. CONCLUDING REMARKS

In this paper, a process to introduce nanoscale cells in homogeneous PEI is presented. The nanofoams produced have a bulk porosity (void fraction) in the range of 25–64%, with the average cell sizes in the range of 40–100 nm. Uniform nucleation of cells throughout the volume of the PEI specimen was observed. Supercritical CO_2 at 20 MPa was used as the blowing agent, and the specimens were foamed in a hot press to ensure flatness for further processing and characterization. The nanostructure is produced in this process by creating conditions for a large number of cells to nucleate in the entire volume of the polymer. This is achieved by first saturating the polymer with CO_2 at 20 MPa pressure. When the PEI specimen is removed from the pressure vessel, it is thermodynamically unstable due to the supersaturation of the dissolved gas. When this specimen is heated close to the glass transition temperature of the gas–polymer system, a large number of cells nucleate.

There are still many unanswered questions. The precise mechanism for cell nucleation is not known. Further, we do not yet understand why at the gas concentration used in this study we see a cell nucleation density $>10^{15}$ cells/cm^3 that leads to the nanostructure observed. By contrast, a 20% lower gas concentration produces cell nucleation that is four orders-of-magnitude smaller, yielding a microcellular structure with cells that are 100 times larger. Is the nanostructure produced closed-cell or is open and interconnected? Can the solid skin on the nanofoam be removed without damaging the core to access the nanostructured polymer? These are all

https://doi.org/10.1557/jmr.2013.108 Published online by Cambridge University Press

the questions we are currently exploring and will be addressed in future communications.

It was found that for the production of nanocellular PEI, the critical process parameters are: desorption time, gas concentration, foaming time, foaming pressure, and foaming temperature. Desorption time strongly affects the development of internal blisters and the size of the resulting transition layer. Blister-free samples may be obtained under the stated conditions with desorption equal to or longer than 35 min. Increased foaming time increases the resultant cell size and relative density but can eliminate the curvature found in samples foamed for shorter times. Finally, the foaming temperature significantly affects the nanostructure of the foam. In one experiment, it was found that when the clamping force is increased from 1 to 10 tons, the average cell size increased from 40 to 4000 nm or by a factor of 100. This points to the clamping force as an important process variable to control the nanostructure introduced in the polymer.

REFERENCES

1. X. Xu, C.B. Park, D. Xu, and R.P. Iliev: Effects of die geometry on cell nucleation of PS foams blown with CO_2. *Polym. Eng. Sci.* **43**, 1378 (2004).
2. S. Siripurapu, J.M. DeSimone, S.A. Khan, and R.J. Spontak: Low-temperature, surface-mediated foaming of polymer films. *Adv. Mater.* **16**, 989 (2004).
3. M. Shimbo, I. Higashitani, and Y. Miyano: Mechanism of strength improvement of foamed plastics having fine cell. *J. Cell. Plast.* **43**, 157 (2007).
4. S.S. Sundarram and W. Li: On thermal conductivity of micro and nanocellular polymer foams. *Polym. Eng. Sci.* (2013).
5. R.W.B. Sharudin and M. Ohshima: CO_2-induced mechanical reinforcement of polyolefin-based nanocellular foams. *Macromol. Mater. Eng.* **296**, 1046 (2011).
6. D.I. Collias, D.G. Baird, and R.J.M. Borggreve: Impact toughening of polycarbonate by microcellular foaming. *Polymer* **35**, 3978 (1994).
7. B. Krause, G-H. Koops, N.F.A. van der Vegt, M. Wessling, M. Wübbenhorst, and J. van Turnhout: Ultralow-k dielectrics made by supercritical foaming of thin polymer films. *Adv. Mater.* **14**, 1041 (2002).
8. J.L. Hedrick, T.P. Russell, J. Labadie, M. Lucas, and S. Swanson: High temperature nanofoams derived from rigid and semi-rigid polyimides. *Polymer* **36**, 2685 (1995).
9. C.B. Park, A.H. Behravesh, and R.D. Venter: Low density microcellular foam processing in extrusion using CO_2. *Polym. Eng. Sci.* **38**, 1812 (2004).
10. D. Miller, P. Chatchaisucha, and V. Kumar: Microcellular and nanocellular solid-state polyetherimide (PEI) foams using sub-critical carbon dioxide I. Processing and structure. *Polymer* **50**, 5576 (2009).
11. J.L. Hedrick, C.J. Hawker, R. DiPietro, R. Jérôme, and Y. Charlier: The use of styrenic copolymers to generate polyimide nanofoams. *Polymer* **36**, 4855 (1995).
12. S. Hongliu and J.E. Mark: Preparation, characterization, and mechanical properties of some microcellular polysulfone foams. *J. Appl. Polym. Sci.* **86**, 1692 (2002).
13. B. Krause, H.J.P. Sijbesma, P. Münüklü, N.F.A. Van der Vegt, and M. Wessling: Bicontinuous nanoporous polymers by carbon dioxide foaming. *Macromolecules* **34**, 8792 (2001).
14. B. Krause, M.E. Boerrigter, N.F.A. Van der Vegt, H. Strathmann, and M. Wessling: Novel open-cellular polysulfone morphologies produced with trace concentrations of solvents as pore opener. *J. Membr. Sci.* **187**, 181 (2001).
15. S.S. Zhang: A review on the separators of liquid electrolyte Li-ion batteries. *J. Power Sources* **164**, 351 (2007).
16. J. Martini, N.P. Suh, and F.A. Waldman: Microcellular closed cell foams and their method of manufacture. Patent #4473665, September 25, 1984. Massechusetts Institute of Technology: USA, 1984.
17. J. Martini, F.A. Waldman, and N.P. Suh: The production and analysis of microcellular thermoplastic foam. *SPE ANTEC Tech. Pap.* **28**, 674 (1982).
18. S. Huang, G. Wu, and S. Chen: Preparation of open cellular PMMA microspheres by supercritical carbon dioxide foaming. *J. Supercrit. Fluids* **40.2**, 323 (2007).
19. V. Kumar and J.E. Weller: A process to produce microcellular PVC. *Int. Polym. Proc.* **8**, 73 (1993).
20. V. Kumar and J. Weller: Production of microcellular polycarbonate using carbon dioxide for bubble nucleation. *J. Eng. Ind.* **116**, 413 (1994).
21. R.E. Murray, J.E. Weller, and V. Kumar: Solid-state microcellular acrylonitrile-butadiene-styrene foams. *Cell. Polym.* **19**, 413 (2000).
22. D.F. Baldwin, C.B. Park, and N.P. Suh: A microcellular processing study of poly (ethylene terephthalate) in the amorphous and semicrystalline states. Part I: Microcell nucleation. *Polym. Eng. Sci.* **36**, 1437 (2004).
23. D.F. Baldwin and N.P. Suh: Microcellular poly (ethylene terephthalate) and crystallizable poly (ethylene terephthalate): Characterization of process variables, in *ANTEC 92–Shaping the Future*, Vol. **1**; Society of Plastics Engineers, 1992; p. 1503-1507.
24. X. Wang, V. Kumar, and W. Li: Low density sub-critical CO_2-blown solid-state PLA foams. *Cell. Polym.* **26**, 11 (2007).
25. S.K. Goel and E.J. Beckman: Generation of microcellular polymers using supercritical CO_2. *Cell. Polym.* **12**, 251 (1993).
26. T.S. Chow: Molecular interpretation of the glass transition temperature of polymer-diluent systems. *Macromolecules* **13**, 362 (1980).
27. T. Nemoto, J. Takagi, and M. Ohshima: Nanoscale cellular foams from a poly (propylene) rubber blend. *Macromol. Mater. Eng.* **293**, 991 (2008).
28. T. Nemoto, J. Takagi, and M. Ohshima: Control of bubble size and location in nano/microscale cellular poly (propylene)/rubber blend foams. *Macromol. Mater. Eng.* **293**, 574 (2008).
29. Y. Fujimoto, S.S. Ray, M. Okamoto, A. Ogami, K. Yamada, and K. Ueda: Well-controlled biodegradable nanocomposite foams: From microcellular to nanocellular. *Macromol. Rapid Commun.* **24**, 457 (2003).
30. B. Krause, K. Diekmann, N.F.A. Van der Vegt, and M. Wessling: Open nanoporous morphologies from polymeric blends by carbon dioxide foaming. *Macromolecules* **35**, 1738 (2002).
31. D. Miller and V. Kumar: Microcellular and nanocellular solid-state polyetherimide (PEI) foams using sub-critical carbon dioxide II. Tensile and impact properties. *Polymer* **52**, 2910 (2011).
32. S.G. Kazarian: Polymer processing with supercritical fluids. *Polymer Sci.* **42**, 78 (2000).
33. D.L. Tomasko, H. Li, D. Liu, X. Han, M.J. Wingert, L.J. Lee, and K.W. Koelling: A review of CO_2 applications in the processing of polymers. *Ind. Eng. Chem. Res.* **42**, 6431 (2003).
34. C. Zhou, N. Vaccaro, S.S. Sundarram, and W. Li: Fabrication and characterization of polyetherimide nanofoams using supercritical CO_2. *J. Cell. Plast.* **48**, 235 (2012).
35. L. Sorrentino, M. Aurilia, and S. Iannace: Polymeric foams from high performance thermoplastics. *Adv. Polym. Tech.* **30**, 234 (2011).
36. J. Crank: *The Mathematics of Diffusion* (Oxford University Press: London, England, 1956), p. 45.

https://doi.org/10.1557/jmr.2013.108 Published online by Cambridge University Press